Relationship between Regional White Matter Hyperintensities and Alpha Oscillations in Older Adults

Authors: Deniz Kumral*[1,2], Elena Cesnaite*[1], Frauke Beyer[1,3], Simon M. Hofmann[1], Tilman Hensch[4,5,6], Christian Sander [4,5], Ulrich Hegerl[7], Stefan Haufe[8,9], Arno Villringer[1,2,10], A. Veronica Witte[1,3,10], Vadim Nikulin[1,11]

[1]Department of Neurology, Max Planck Institute for Human Cognitive and Brain Sciences, Leipzig, Germany
[2]Berlin School of Mind and Brain, Humboldt-Universita t zu Berlin, Berlin, Germany
[3]CRC Obesity Mechanisms, Subproject A1, University of Leipzig, Leipzig, Germany
[4]Department of Psychiatry and Psychotherapy, University of Leipzig Medical Center, Leipzig, Germany
[5]LIFE – Leipzig Research Center for Civilization Diseases, University of Leipzig, Leipzig, Germany
[6]IUBH International University, Erfurt, Germany
[7]Department of Psychiatry, Psychosomatics and Psychotherapy, Goethe University Frankfurt, Frankfurt, Germany
[8]Berlin Center for Advanced Neuroimaging, Charité – Universitätsmedizin Berlin, Berlin, Germany
[9]Bernstein Center for Computational Neuroscience Berlin, Berlin, Germany
[10]Clinic of Cognitive Neurology, University Hospital Leipzig, Leipzig, Germany
[11]Centre for Cognition and Decision Making, Institute of Cognitive Neuroscience, National Research University Higher School of Economics, Moscow, Russian Federation

* These authors contributed equally to the manuscript.

Corresponding Author: Deniz Kumral, dkumral@cbs.mpg.de, Department of Neurology, Max Planck Institute for Human Cognitive and Brain Sciences, Leipzig, Germany, Stephan Str.1a, 04103, Leipzig, German

Abstract

White matter hyperintensities (WMHs) in the cerebral white matter and attenuation of alpha oscillations (AO; 7–13 Hz) occur with the advancing age. However, a crucial question remains, whether changes in AO relate to aging *per se* or they rather reflect the impact of age-related neuropathology like WMHs. In this study, using a large cohort (N=907) of elderly participants (60-80 years), we assessed relative alpha power (AP), individual alpha peak frequency (IAPF) and long-range temporal correlations (LRTC) from resting-state EEG. We further associated these parameters with voxel-wise WMHs from 3T MRI. We found that higher prevalence of WMHs in the superior and posterior corona radiata was related to elevated relative AP, with strongest correlations in the bilateral occipital cortex, even after controlling for potential confounding factors. In contrast, we observed no significant relation of probability of WMH occurrence with IAPF and LRTC. We argue that the WMH-associated increase of AP reflects generalized and likely compensatory changes of AO leading to a larger number of synchronously recruited neurons.

Key words: EEG, MRI, white matter hyperintensity, aging, alpha power

Word count: 167 words

1. Introduction

White matter lesions (WML) are highly prevalent in the elderly and are of paramount clinical relevance since they are known to accompany cognitive decline and dementia (Birdsill et al., 2014; Debette and Markus, 2010; Habes et al., 2016). WML are considered to reflect mainly small vessel disease (Wardlaw et al., 2015), which typically affects periventricular regions and deep white matter sparing U-fibers (Habes et al., 2016). Little is known, however, whether and how WML impact functional measures of brain activity. Due to their location, white matter hyperintensities (WMHs) may cause disconnection of neuronal populations (O'Sullivan et al., 2001). Theoretically, such damage of cortico-cortical and cortico-subcortical pathways is expected to alter synchronized activity of neurons measured with M/EEG (Hindriks and van Putten, 2013).

One of the most prominent EEG rhythms are alpha oscillations (AO), which have been shown to originate from thalamo-cortical and cortico-cortical interactions (Bazanova and Vernon, 2014; Lopes Da Silva et al., 1997). Importantly, measures of AO have been related to many aspects of sensory and cognitive function (Fox et al., 2016; Klimesch, 1999) and to endophenotypes of brain aging (Ishii et al., 2018; Knyazeva et al., 2018) either using power or individual alpha peak frequency (IAPF). Apart from these two measures of AO, temporal dynamics of the signal can be assessed with long-range temporal correlations (LRTC; Linkenkaer-Hansen et al., 2001). LRTC indicate the presence of scale-free neuronal dynamics, when fluctuation patterns of the signal are similar at different time scales. Power-law decay of LRTC is consistent with the idea of neuronal networks operating at a critical state, — characterized by a balance between inhibition and excitation (Shew and Plenz, 2013), — which may be beneficial for information processing and storage (Mahjoory et al., 2019; Samek et al., 2016; Smit et al., 2011).

As both static (power, IAPF) and dynamic (LRTC) measures of AO might be affected by microstructural deteriorations, due to the disconnection among neural cells and damage to cortico-cortical and cortico-subcortical pathways (Madden et al., 2017), WML-associated alterations of EEG rhythms are plausible. However, there are only few EEG studies that have directly investigated the relationship between AO and WML or integrity (Babiloni et al., 2011, 2008a; Valdés-Hernández et al., 2010; van Straaten et al., 2012). Previously, local and global disturbances of brain anatomy like WM microstructure (Hinault et al., 2020; Hindriks et al., 2015; Minami et al., 2020; Valdés-Hernández et al., 2010) have been found to be related to alpha rhythm affecting its peak frequency and power. For instance, a study by (Valdés-Hernández et al., 2010) provides evidence that peak frequency can be associated with both decrease and increase (depending on the region) in the microstructure of thalamocortical or corticothalamic fibers assessed by Fractional Anisotropy (FA) using diffusion tensor imaging (DTI). Interestingly, so far only a few studies have investigated the relationship between AO and WML (Babiloni et al., 2009, 2008b, 2008a). However, to our knowledge, no link between voxel-wise whole-brain WMHs and AO has been investigated. Moreover, a crucial question still remains unresolved, for example whether changes in AO relate to aging *per se* or rather they represent the impact of age-related neuropathology, for instance, WML. In this study, using a large population-based sample of elderly individuals, we hypothesized that WMHs affect the parameters (AP, IAPF, LRTC) of AO in a topographically specific manner. We further postulated that this effect might be independent of age.

2. Methods

2.1.Participants

Participants were drawn from the population-based Leipzig Research Center for Civilization Diseases LIFE-Adult study (Loeffler et al., 2015). All participants provided written informed consent, and the study was approved by the ethics committee of the medical faculty at the University of Leipzig, Germany. The study was performed in agreement with the Declaration of Helsinki. A subset of participants underwent a 3-Tesla MRI head scan and resting state (rs)EEG recordings on two separate assessment days. We selected participants above 60 years of age and without additional brain pathology or history of stroke, multiple sclerosis, epilepsy, Parkinson's disease, intracranial hemorrhage, or brain tumors. We further excluded individuals whose rsEEG recordings were not temporally close to the MRI acquisition time and participants for whom alpha peak could not be identified. This resulted in a final sample of 907 participants (M=69.49 ± 4.63, 380 female) for the rsEEG sensor space analysis. After excluding individuals with failed T1-weighted segmentation and head-modeling, the final sample for the rsEEG source analysis was 855 (M=68.89 ± 4.66, 360 female). For a detailed overview of the selection process, see **Figure 1**.

Figure 1 – Flow chart visualizing the selection process of the MRI and EEG sample.

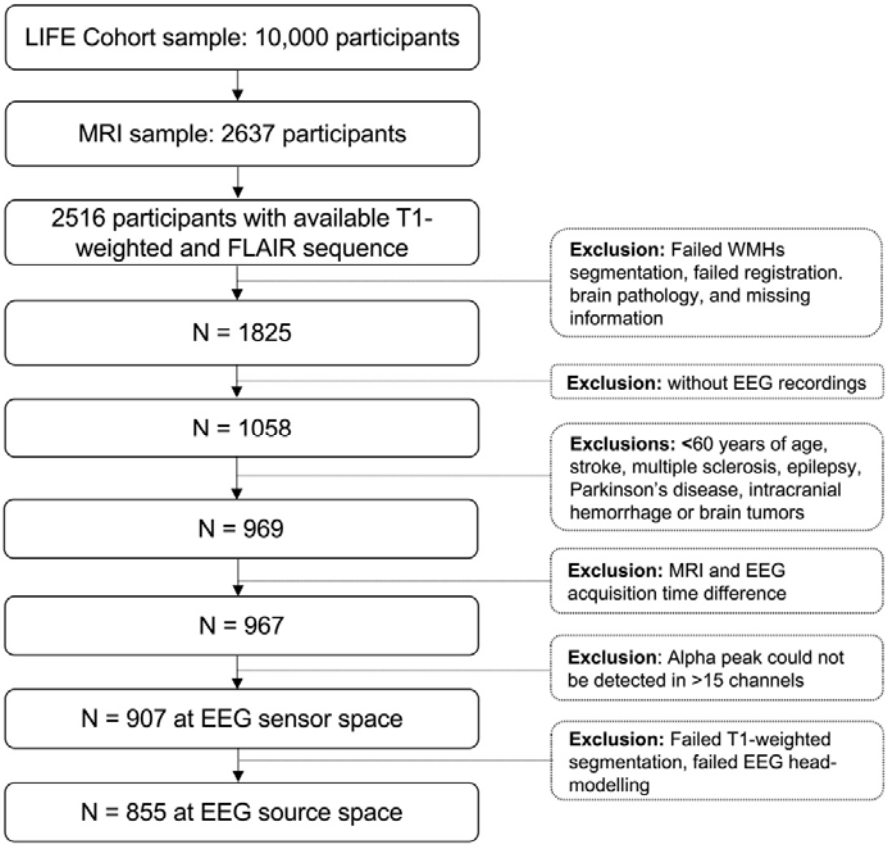

2.2.MRI Acquisition and Processing

All MRI scans were performed at 3 Tesla on a MAGNETOM Verio scanner (Siemens, Erlangen, Germany). The body coil was used for radiofrequency (RF) transmission and a 32- channel head coil was used for signal reception. T1-weighted MPRAGE and FLAIR images were acquired as part of a standardized protocol: MPRAGE (flip angle (FA) = 9°, relaxation time (TR) = 2300 ms, inversion time (TI) = 900 ms, echo time (TE) = 2.98 ms, 1-mm isotropic resolution, acquisition time (AT) = 5.10 min); FLAIR (TR = 5000 ms, TI = 1800 ms, TE = 395 ms, 1x0.49x0.49-mm resolution, AT = 7.02 min).

The automated assessment of WMHs was computed in a previous study(Lampe et al., 2019). All images were checked by a study physician for incidental findings. A computer-

based WMHs segmentation algorithm was then used to automatically determine WMH volume on T1-weighted MPRAGE and FLAIR images (Shiee et al., 2010) and inspected visually for segmentation errors. Binary WMH maps of all participants were nonlinearly co-registered to a standardized MNI template (1-mm isometric) with ANTS (Avants et al., 2011). In standard space, binary subject-wise WMH maps were grand-averaged to create a population WMH frequency map (Jenkinson et al., 2012). As previously implemented (Lampe et al., 2019), to segregate the periventricular (pv)WMH and deep (d)WMH, a default distance of 10 mm to the ventricular surface was used (DeCarli et al., 2005). Every voxel of WMH located within this border was classified as pvWMH; voxels outside the border were classified as dWMH. Regional WMH volume was calculated separately for the deep and periventricular WM. We added a constant value 1 to every participant's regional dWMH volume because there were participants without lesions in the deep WM (Lampe et al., 2019). We then calculated the ratio of dWMH and pvWMH (dWMH/pvWMH) as localized WMH volume.

2.3.EEG Acquisition and Preprocessing

RsEEG activity was recorded in an electrically and acoustically shielded room using an EEG cap with 34 passive Ag/AgCl electrodes (EasyCap, Brain Products GmbH, Germany). 31 scalp electrodes were placed according to the extended international 10–20 system. The signal was amplified using a QuickAmp amplifier (Brain Products GmbH, Germany). Two electrodes recorded vertical and horizontal eye movements while one bipolar electrode was used for electrocardiography. The rsEEG activity was referenced against common average and sampled at 1000 Hz with a low-pass filter of 280 Hz. Impedances were kept below 10 kΩ. RsEEG data were preprocessed using EEGLAB toolbox (version 14.1.1b) and scripts were custom written in Matlab 9.3 (Mathworks, Natick, MA, USA). We filtered data between 1 and 45 Hz and applied a notch filter at 50 Hz. We then down-sampled the

data to 500 Hz and ran a semi-automatic pipeline for artifact rejection: different noise threshold levels to mark bad time segments were used for the signal filtered in higher frequency (15–45 Hz) and lower frequency (1–15 Hz) ranges. The noise threshold for higher frequencies was set to 40 μV since noise at this range (i.e., induced by muscle activity) is typically lower in amplitude. The noise threshold for the lower frequency range was set to + 3SD over the mean amplitude of a filtered signal between 1 and 15 Hz. To control for the accuracy of automatically marked bad segments, we compared them to the noisy segments marked by another research group (Jawinski et al., 2017). Whenever these segments did not overlap by more than 10 s or they exceeded 60 s of total bad-segment duration, we inspected those datasets visually (~10% of cases) to confirm whether they indeed were contaminated by noise. We further visually assessed power spectral densities (PSD) for data quality and used it to identify broken channels. Next, using independent component analysis (Infomax; Bell and Sejnowski, 1995), activity associated with the confounding sources—namely eye-movements, eye-blinks, muscle activity, and residual heart-related artifacts—was removed.

2.4.EEG Sensor Space Analysis

2.4.1. Parameters of Alpha Oscillations

For rsEEG analysis, we used the first 10 min of a recording in order to avoid the potential effect of participants' drowsiness. We individually adjusted the alpha band frequency range by locating a major peak between 7 and 13 Hz on Welch's PSD with 4-s Hanning windows. Thus, we determined individual alpha peak frequency (IAPF) in every channel and defined a bandwidth not exceeding 3 Hz around the peak. We then calculated relative AP for the individually adjusted alpha frequency range dividing it by the broadband power calculated in the 3–45-Hz frequency range. LRTC were calculated using detrended fluctuation analysis on the amplitude envelope (calculated with Hilbert transform) of alpha band oscillations in time windows ranging from 3 to 50 seconds (while respecting the

boundaries where the bad segments had been cut) based on the previously published procedure (Hardstone et al., 2012). Here, the scaling exponent (ν) is a measure of the LRTC in the signal. An exponent of 0.5 reflects uncorrelated signals (i.e., resembling white noise), while an exponent between $0.5<\nu<1$ shows persistent autocorrelation and thus the presence of LRTC (Hardstone et al., 2012). The presence of LRTC indicates that past neuronal events are likely to affect neuronal activity in the future even when these events are separated by tens of seconds. The illustration of parameters of AO are shown in **Figure 2**.

To reduce data dimensionality of rsEEG sensor space data used for the whole-brain voxel-wise inference analyses, we further grouped EEG channels into six coarser brain regions (frontal, central, temporal, parietal, and occipital), as shown in **Figure 3A**.

Figure 2– Illustration of parameters of alpha oscillations. A) Resting state EEG time series data (blue) consists of various frequency bands that can be defined by their power and peak frequency. **B)** The temporal dynamics of a signal filtered in alpha frequency range (8–12 Hz) is assessed by the properties of its amplitude envelope (red) using long-range temporal correlations (LRTC). Scaling exponent (ν) quantifies the presence of LRTC.

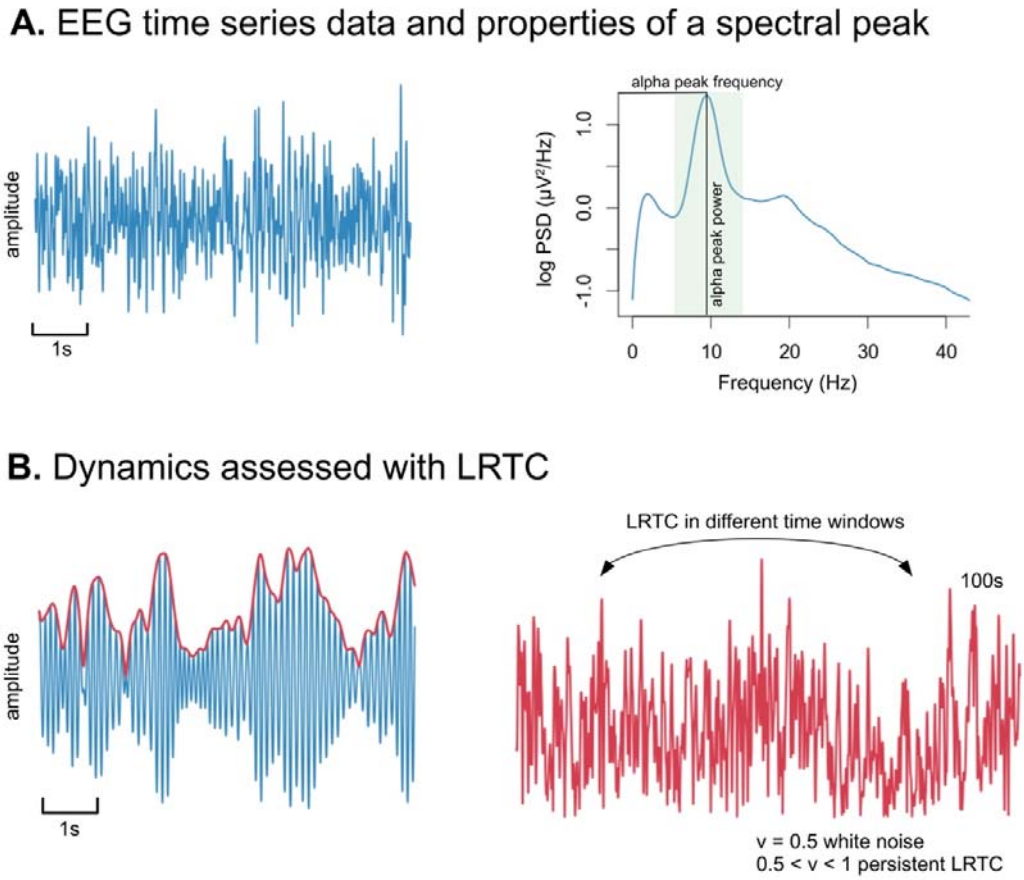

139

140 **2.5.EEG Source Space Analysis**

141 To reconstruct sources of the rsEEG signal, we calculated leadfield matrices based on
142 individual brain anatomies and standard electrode positions. The T1-weighted MPRAGE
143 images were segmented using the Freesurfer v.5.3.0 software (Fischl, 2012). We constructed
144 a 3-shell boundary element model (BEM) which was subsequently used to compute the
145 leadfield matrix using OpenMEEG (Gramfort et al., 2010). Approximately 2,000 cortical
146 dipolar sources were modeled for each individual. Source reconstruction was performed
147 using exact low resolution brain electromagnetic tomography (eLORETA; Pascual-Marqui,
148 2007) with a regularization parameter of 0.05. We filtered the signal within the individually
149 adjusted alpha frequency band range as well as in broadband range (3–45 Hz), squared it, and
150 summed up across all three dipole directions. Relative AP was then calculated in each voxel

through the division of AP by the broadband power. The cortex surface mantle was divided into 68 regions of interest (ROIs) based on the Desikan-Killiany atlas (Desikan et al., 2006). These were further combined into five coarser ROIs (frontal, parietal, temporal, occipital, and cingulate) for the right and left hemispheres following a standard parcellation atlas, as shown in **Figure 3B**. Relative AP values were averaged across each ROI.

Figure 3 – Illustration of the regions of interest (ROIs) identified for EEG. Schematic topography for resting state EEG in **A)** sensor space and **B)** source space. ROIs that form the frontal region are in purple, central region and cingulate region (source) in orange, temporal region in yellow, parietal region in green, and occipital region in blue.

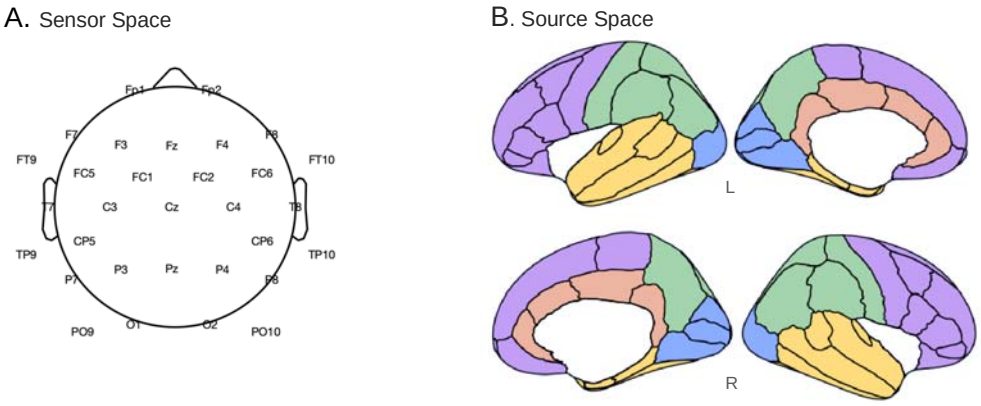

2.6.Statistical Analyses

2.6.1. Correlation of Age with WMH Volume and Alpha Oscillations

Pearson correlations were calculated to examine the relationship between i) age and total and regional WMH volume (dWMH/pvWMH) and ii) the parameters of AO in six regions at sensor space. Differences between correlations were assessed with Fisher's r-to-z transformation implemented in R version 3.5.2 (http://www.R-project.org/). To correct for multiple comparisons, p-values were then adjusted using the False Discovery Rate (FDR; Hochberg, 2016).

2.6.2. Topographical Relevance Analyses of WMHs for Alpha Oscillations at Sensor Space

To identify regions in which WMHs robustly correlated with AO, we performed whole-brain voxel-wise regressions. More precisely, we applied general linear models (GLMs) in which individual values of IAPF, relative AP, and LRTC were used as predictors for the topographical occurrence of WMHs, adjusting for effects of age, sex, and intracranial volume (ICV) as covariates of no interest. 3D voxel-wise binary lesion maps were analyzed using FSL's randomize (Winkler et al., 2014). For each statistical analysis, positive and negative contrasts were computed. Significance of results was based on threshold-free cluster enhancement (TFCE, N=10,000 permutations) with family-wise error (FWE) corrected p-values of $p<0.05$. We further reported statistical results for the more conservative FWE threshold of $p<0.005$.

2.6.3. Topographical Relevance Analyses of WMHs for Alpha Power at Source Space

To assess the association between relative AP and whole-brain WMHs, we implemented GLMs separately for 10 ROIs with relative AP as covariate of interest, and age, sex, and ICV as covariates of no interest. Because we found a positive correlation between the voxel-wise occurrence of WMHs and relative AP at the sensor space, we only computed a

positive contrast. All statistical analyses were further corrected for multiple comparisons using TFCE based permutation testing (N=10,000) at FWE level of $p<0.05$, as well as with a conservative threshold of $p<0.005$.

2.7.Sensitivity Analyses

2.7.1. Control for Confounding factors

Given that different cardiovascular risk factors including body mass index (BMI), systolic blood pressure (SBP), smoking, and diabetes are associated with WMHs (Habes et al., 2016; Lampe et al., 2019; Ryu et al., 2014), we further considered these factors as potential confounders (as covariates of no interest) for the voxel-wise associations between parameters of AP and probability of WMH occurrence in the overall sample (N=907). To assess a degree of collinearity between the regressors used in GLMs, we additionally computed variance inflation factor (vif) in R. All predictors had a vif score below 2, therefore, we concluded that models showed acceptably low multicollinearity.

2.7.2. Medication

We implemented the voxel-wise inference analyses between parameters of AO and WMHs excluding participants taking medications affecting the central nervous system (opioids, hypnotics and sedatives, anti-parkinsonian drugs, anxiolytics, anti-psychotics, anti-epileptic drugs). The resulting sample included 801 individuals ($M=68.96 \pm 4.58$, 323 female).

2.7.3. Control Analyses

To assess the robustness of our results, we further applied voxel-wise inference analyses between the probability of WMH occurrence and absolute AP in the left and right occipital region at EEG source space, using age, sex, and ICV as covariates of no interest. Absolute power in both regions was log transformed to normalize the distribution of the data for statistical analyses.

2.8. Mediation Analyses

We performed mediation analyses using *mediation* package (Tingley et al., 2014) in R to examine whether total or localized WMH (dWMH/pvWMH) volume mediates the relationship between age as an independent and AO at sensor space as a dependent variable. We computed 99% confidence intervals (CI) using bootstrapping (5,000) for all inferences. Indirect effects, and the sum of the indirect effects were considered significant if the CI did not contain zero. Here, direct and mediation effects are called average direct effect (ADE) and average causal mediation effect (ACME, also referred to as indirect effect), respectively. Statistically, total effect is the sum of ACME and ADE. The ACME shows whether age was associated with parameters of AO through a mediator.

3. Results

3.1.Sample Characteristics

Details about the demographic, anthropometric, cardiovascular measures, as well as WMH volume, and AO can be found in *Table 1*. Histograms of total WMH volume, averaged relative AP, IAPF, and LRTC across channels can be found in Supplementary Figure 1.

Table 1 – Sample Characteristics

	Mean or n	Min.	Max.	SD
Age (in years)	69.49	60.15	80.03	4.63
Female / Male	380 / 527			
BMI (kg/m^2)	27.59	18.68	42.26	3.97
SBP (mmHg)	133.71	92.00	200.5	16.31
DBP (in mmHg)	74.54	43.5	120	9.06
Never / former / active smokers	517 / 319 / 71			
Diabetes (yes / no / unknown)	748 /143 / 16			
WMH volume (mm3)	3935	127	78509	6676.76
dWMH/pvWMH (%)	0.44	0.01	3.64	0.40
ICV (mm3)	1729811	1297219	2466529	147492.5
Mean Rel. AP (%)	0.55	0.21	0.88	0.15
Mean IAPF (Hz)	9.4	7.34	12.01	0.86
Mean Scaling Exponent (*v*)	0.73	0.53	1.14	0.093

Abbreviations.: Rel. AP = Relative Alpha Power; BMI = body mass index; DBP = diastolic blood pressure; dWMH/pvWMH = the ratio of deep/periventricular white matter hyperintensities; SD = standard deviation; ICV = intracranial volume; IAPF = individual alpha peak frequency; SBP = systolic blood pressure; WMH = white matter hyperintensity

3.2.Topography and Characteristics of Alpha Oscillations

The relative AP at sensor space showed a maximum over the occipital channels, with a mean value of 0.66 ± 0.17. Similarly, the relative AP at source space showed a maximum over the bilateral occipital cortex, including cuneus and lateral occipital regions with a mean value of 0.59 ± 0.18. The grand-average IAPF was 9.40 ± 0.49 Hz, showing larger values at occipital regions. The average scaling exponent (*v*) was 0.72 ± 0.017. Similarly, topographies of the scaling exponent had higher values at occipital and parietal areas as well as frontal regions (Supplementary Figure 2).

3.3.Correlations

3.3.1. Association of Age with WMH Volume and Alpha Oscillations

We found a correlation between age and total WMH volume ($r=0.374$, $p<0.001$), but not with the dWMH/pvWMH ($p>0.05$). Regarding parameters of AO, we found that higher age was associated with decreased IAPF in all EEG ROIs (r from -0.13 to -0.17, $p_{FDR}<0.05$), while no correlations between age and relative AP or LRTC were found (all $p_{FDR}>0.05$). A

full report of these correlations for the entire sample and by sex are provided in Supplementary Figures 3–7.

3.3.2. Topographical Association Between WMHs and Alpha Oscillations at Sensor Space

The voxel-wise inference analyses revealed that higher relative AP in the frontal region was correlated with higher WMH probabilities in the right body of corpus callosum ([16, -26, 32], T=3.76, k=653). Higher relative AP in the central region was associated with higher WMH probabilities in the right anterior thalamic radiation extending to the posterior corona radiata ([22, -49, 37], T = 4.44, k=2,744), while higher relative AP in the right temporal region was linked to higher WMHs in the right superior longitudinal fasciculus ([22, -49, 37], T=4.52, k=6,893) extending to the left inferior fronto-occipital fasciculus ([-21, -53, 32], T=4.00, k=4,210). Furthermore, higher relative AP in the parietal region was associated with higher WMHs in the right superior corona radiata ([18, -19, 37], T=4.05, k=4,474). Similarly, for relative AP in the occipital region, we observed a higher prevalence of WMHs in the bilateral superior corona radiata through the body of the corpus callosum to the anterior corona radiata, including the right anterior thalamic radiation ([18, -19, 37], T=4.39, k=9,450). Accordingly, higher voxel-wise WMH probabilities were associated with higher relative AP independent of age, sex, and brain size, as shown in **Figure 4**. Note that using a more stringent FWE rate of $p < 0.005$, correlation between probability of WMH occurrence and relative AP was only evident for the occipital region ([18, -19, 37], T=4.39, k=904). Finally, no associations between voxel-wise WMHs and IAPF or LRTC were observed ($p>0.05$).

Figure 4 – Association between regional white matter hyperintensities (WMHs) and relative alpha power (AP) at EEG sensor space. A) Voxel-wise correlation between probability of WMH occurrence and relative AP in the EEG frontal region (purple), central region (orange), right temporal region (yellow), parietal region (green), and occipital region (blue). The significant clusters based on whole-brain voxel-wise inference analyses (TFCE, FWE-corrected, $p < 0.05$). **B)** Scatter plots show the positive association between relative AP. The resulting statistical images (P-map) were further thresholded at 0.05 and binarized. Abbreviations.: A = anterior; L = left; R = right; P = posterior

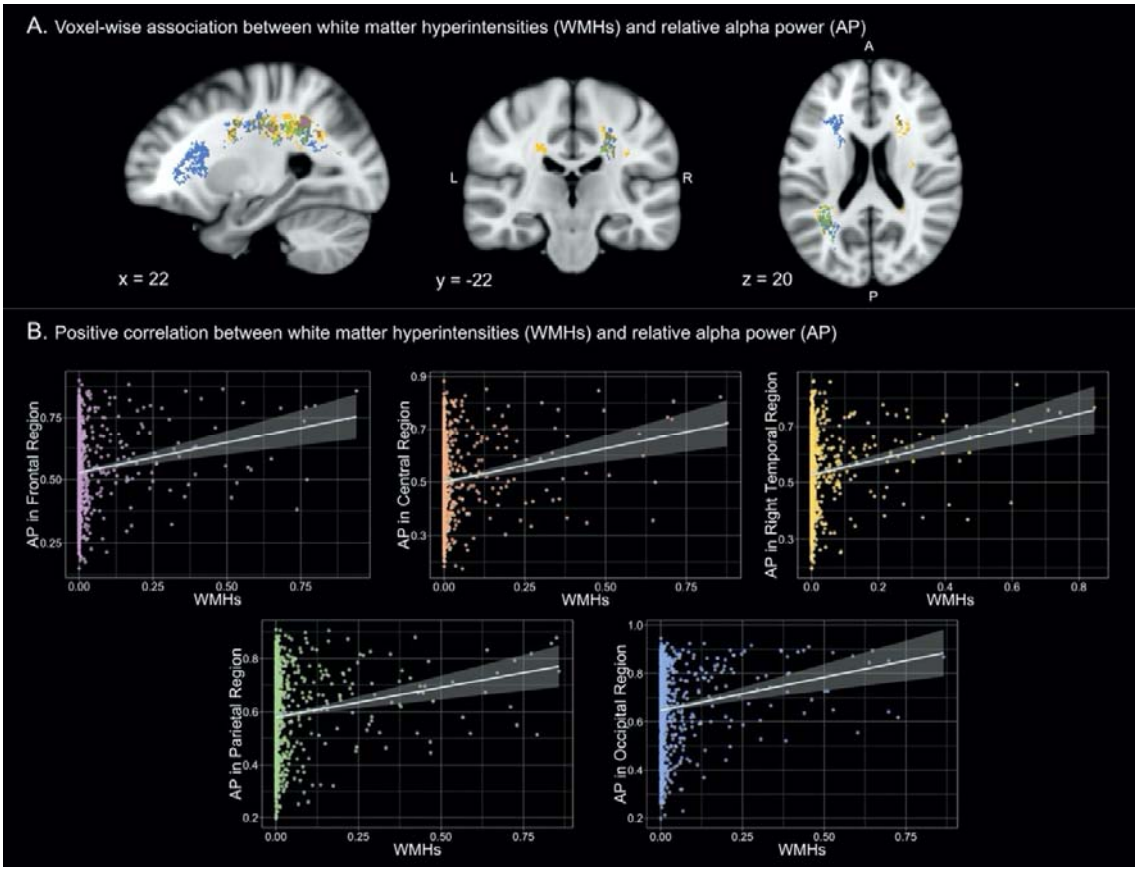

3.3.3. Topographical Association Between WMHs and Alpha Oscillations at Source Space

We found that higher relative AP in all EEG regions except for the left frontal region was associated with higher probability of WMH occurrence (*Table 2*). With the stricter FWE-level of $p<0.005$, the association between the occurrence of WMHs and relative AP was evident for left ([18, -19, 37], $T=4.29$, $k=192$) and right occipital regions ([18, -19, 37], $T=4.45$, $k=845$).

Table 2 – Positive correlation between the probability of white matter hyperintensity (WMH) occurrence and relative alpha power (AP) at EEG source space. Peak voxel MNI coordinates (x, y, z) and cluster size (k) for the association between WMHs probability and relative AP for five regions of interest for each hemisphere at source space across 855 elderly participants (TFCE, $p < 0.05$, FWE-corrected).

EEG Region	MRI Region	x	y	z	k	T-value
Left Frontal	Right Posterior Corona Radiata / Right Anterior Thalamic Radiation	21	-46	36	219	4.38
Right Cingulate	Right Anterior Thalamic Radiation / Right Anterior Thalamic Radiation	22	-49	37	2310	4.33
	Left Superior Corona Radiata	-22	6	31	655	4.29
	Right Superior Corona Radiata	29	-46	26	359	3.65
Left Cingulate	Right Anterior Thalamic Radiation / Superior Longitudinal Fasciculus	22	-49	37	3280	4.44
	Left Superior Corona Radiata	-22	6	31	597	4.33
Right Temporal	Right Anterior Thalamic Radiation	20	-50	36	4669	4.57
	Left Anterior Corona Radiata	-18	18	27	2044	4.14
	Right Inferior Fronto-occipital Fasciculus	34	-49	0	129	3.68
Left Temporal	Right Anterior Thalamic Radiation	20	-50	36	602	4.63
	Body of Corpus Callosum	16	-5	36	279	3.63
	Right Posterior Corona Radiata	19	-30	35	132	4.13
Right Parietal	Right Anterior Thalamic Radiation	20	-50	36	3983	4.72
	Left Superior Corona Radiata	-19	11	28	824	3.98
	Left Superior Longitudinal Fasciculus	-24	-12	40	210	4.12
Left Parietal	Right Superior Corona Radiata/Left Corticospinal Tract	19	-25	36	634	3.91
	Right Anterior Thalamic Radiation	20	-50	36	618	4.75
Right Occipital	Right Superior Corona Radiata	18	-19	37	8339	4.45
	Left Superior Corona Radiata	-19	9	29	1070	4.41
	Left Posterior Corona Radiata/Anterior Thalamic Radiation	-24	-27	31	100	3.94
Left Occipital	Right Superior Corona Radiata	18	-19	37	7304	4.29
	Left Superior Corona Radiata	-19	9	29	450	4.19
	Right Inferior Fronto-occipital Fasciculus	34	-37	-4	175	3.94
	Left Superior Corona Radiata	-20	-6	32	133	3.66

3.4.Sensitivity Analyses

3.4.1. Control for Confounding Factors

Voxel-wise inference analyses after controlling for age, sex, ICV, BMI, SBP, diabetes, and smoking status yielded a similar relationship between higher WMH probability and elevated relative AP in the following regions: central ([22, -49, 37], T=4.46, k=5417), right temporal ([22, -49, 37], T=4.52, k=5,417), left temporal ([22, -49, 37], T=4.59, k=4772), parietal ([18, -19, 37], T=3.68, k=231), and occipital ([18, -19, 37], T=4.08, k=4,018) EEG regions across the overall sample. Note that with TFCE, FWE-corrected, $p<0.005$, we did not find any clusters. Lastly, no WMH clusters were related to IAPF or LRTC ($p>0.05$).

3.4.2. Medication

Voxel-wise inference analyses excluding individuals taking central nervous system medication still indicated the association between higher prevalence of WMHs and increased relative AP at sensor space in the following regions: frontal ([17, 9, 31], T=4.42, k=6,880), central ([20, -30, 35], T= 4.46, k=9,063), right temporal ([20, -48, 35], T=4.57, k=12,098), left temporal ([22, -49, 37], T=4.61, k=9,408), parietal ([14, -8, 31], T=4.61, k=9,054), and occipital ([18, -19, 37], T=4.44, k=12,885) EEG regions. Importantly, with TFCE, FWE-corrected, $p<0.005$, we identified WMHs clusters (k>2,000) for occipital, left temporal, right temporal, and a small cluster (k>200) for parietal and central EEG regions. Additional voxel-wise inference analyses revealed that higher WMHs resulted in decreased IAPF in right temporal ([17, -27, 33], T=4.00, k=138) and left temporal regions ([17, -27, 33], T=4.12, k=503). Lastly, no WMHs clusters were related to LRTC ($p>0.05$).

3.4.3. Control Analyses

Voxel-wise inference analyses with absolute AP similarly indicated that higher probability of WMH occurrence was associated with elevated absolute AP in right ([-23, 0, 36], T=3.98, k=5,633) and left occipital regions ([-23, 0, 36], T=4.05, k=5,358).

3.5.Mediation Analyses

We examined whether a total or localized (dWMH/pvWMH) WMH volume could mediate the relationship between age and relative AP, IAPF, and LRTC in all ROIs. Investigating the relationship between age and relative AP, we observed a significant indirect effect (i.e., ACME) of total WMH volume, while ADE and total effect were not significant for most of the regions (99% |CI| > 0, Supplementary Table 1). Only in the right temporal region at sensor space did the total effect of age on relative AP appear to be significant ($p<0.05$), indicating specific pathways between age and relative AP through total WMH volume. Further, we confirmed the indirect effects of total WMH volume for relative AP at EEG source space for left parietal ($\beta=0.0012$, CI = [0.00006-0.002]), left ($\beta=0.0014$, CI = [0.00013-0.002]) and right occipital ($\beta=0.0014$, CI = [0.00015-0.0028]) regions. Finally, our results further revealed that neither total nor localized WMH volume mediated the association of age with IAPF and LRTC at sensor space (all $p>0.05$).

4. Discussion

The main goal of this study was to investigate whether regional WMHs affect parameters of alpha oscillations independently from age. We pursued this aim using a large sample of healthy older individuals from a population-based study (Loeffler et al., 2015). We showed distinct regional relationships between relative AP and WMHs: our topographical analysis suggested that higher occurrence of WMHs in superior, posterior to anterior corona radiata through the body of corpus callosum was related to higher relative AP, with strongest correlations in the bilateral occipital cortex. Adjusting for potential confounding factors including age and cardiovascular risk factors did not change these results.

Alpha rhythm is the most salient rsEEG oscillatory phenomenon that originates from thalamo-cortical and cortico-cortical interactions (Bazanova and Vernon, 2014; Lopes Da Silva et al., 1997). Alterations in AO have previously been linked to changes in different anatomical features including properties of WM (e.g., Valdés-Hernández et al., 2010). Regarding WMHs, for instance, a previous EEG-MRI study showed that higher relative AP in parietal regions was associated with higher scores of the prevalence of WMLs in 79 individuals with mild cognitive impairment (Babiloni et al., 2008a), consistent with our findings in this population-based sample. Previous studies with computational models have given further support for the notion that resonance properties of feedforward, cortico-thalamo-cortical, and intra-cortical circuits largely influence AO (Hindriks and van Putten, 2013). In the present study, we similarly observed that regional WMHs, detected mostly in superior corona radiata, containing thalamo-cortical fibers, affect inter-individual differences in relative AP. Since damage to fibers of the superior corona radiata—connecting the basal ganglia and thalamus to the superior frontal gyrus—is known to be associated with cognitive dysfunction (Leunissen et al., 2014), it is likely that such an elevated AP may be triggered to recruit compensatory neuronal resources to maintain cognitive functioning. But, how could

lesions in the WM possibly affect EEG signal which mainly reflects neural synchrony within gray matter? While in principle a hyperintensity in T2-weighted MR sequences is a quite unspecific marker of various pathologies, postmortem histopathological studies of elderly subjects with WML have mostly reported demyelination, axonal loss, and other consequences of ischemic small vessel disease (Smith et al., 2000; Wardlaw et al., 2015). Myelin contributes to the speed of impulse conduction through axons, and the synchrony of impulses between distant cortical regions (Fields, 2015, 2008). Reductions of conduction velocity due to demyelination and loss of (communicating) axons are assumed to be responsible for cognitive dysfunctions which are known to be based on delicately orchestrated propagations of neuronal signals. Electrophysiologically, interactions and synchrony between neuronal populations are reflected in rhythmic M/EEG signals, of which AO are the most prominent ones (Bazanova and Vernon, 2014; Lopes Da Silva et al., 1997). AP is a quantitative marker of the degree of synchrony in the neuronal activity of the corresponding neuronal populations (Pfurtscheller and Lopes Da Silva, 1999). While for a long-time AO were regarded as idle rhythms of non-active brain areas, a plenitude of studies has convincingly demonstrated that AO play an important role in many cognitive functions (Fox et al., 2016; Klimesch, 1999). For instance, in motor and sensory domains it has been shown that amplitude decreases of AO in focal areas (i.e., reflecting cortical activation) is in turn associated with the inhibition of neighboring cortical areas. This phenomenon is thought to result from a reciprocal relationship between thalamo-cortical and reticular nucleus cells on which the generation of AO is based (Suffczynski et al., 2001). Such topographically specific relationships are likely to be disturbed by alterations in conduction velocity and axonal loss in the thalamo-cortical circuitry. A consequence is a less precise and more generalized (i.e., compensatory; e.g., Cabeza et al., 2018) spread of AO across the cortex leading to a larger number of

synchronously recruited neurons and correspondingly to larger AP. This in turn might explain a positive association between AP and WMHs.

In our study, we did not find strong evidence for age-related attenuations of relative AP, in line with other recent studies (Sahoo et al., 2020; Scally et al., 2018). This could be due to the narrow age range of our participants, as well as the individually adjusted alpha frequency range based on the IAPF. In fact, preserved peak power at IAPF has recently been reported in an older sample (Scally et al., 2018), suggesting that any observed age-dependent power changes might be due to shifts in the frequency range at which alpha peak occurs. Noteworthy, mediation analysis in the current study indicated that the influence of higher age to elevated relative AP (in the right temporal region) was mediated by the higher total WMH volume.

In the literature, other commonly reported age-dependent changes in spectral parameters of EEG include slowing of the alpha peak (Knyazeva et al., 2018). We replicated the slowing of the IAPF with increasing age despite the narrow age range. Alpha peak slowing has previously been suggested to be linked to a less efficient coordination of neuronal activity in this frequency range (Mierau et al., 2017). We further explored the relationship between age and LRTC in the amplitude envelope of AO that represents scale-free modulation of resting state oscillations. LRTC have previously been linked to the presence of a critical state in neural networks, which is characterized by the balance of excitation and inhibition (Poil et al., 2012). Regarding the association between age and LRTC, previous studies have shown that the observed age-related changes might be dependent on age range—it increases from childhood to early adulthood, after which it stabilizes (Nikulin and Brismar, 2005; Smit et al., 2011). In accordance with these previous findings, in our sample of elderly subjects we observed no pronounced age-related LRTC

404 attenuations, which is consistent with relatively stable dynamic properties of neuronal
405 oscillations at higher age.

5. Limitations

While a strength of this study is in the large population-based sample, one of the limitations is in investigating only *cortical* oscillations. An interesting direction for future research would be to study generators of oscillations in deep brain structures (e.g., thalamus) and how they propagate through WM pathways, especially when these pathways are affected. Research using other advanced techniques such as quantitative MRI or specific assessment of tissue properties with ultra-high field MRI combined with intracranial EEG recording could further provide valuable insights into the nature of the relationship between WM properties and AO. Lastly, we performed a relatively coarse parcellation of the brain at EEG source space analysis due to the relatively small number of electrodes (n=31). A denser spatial sampling of the EEG (not available in the present cohort) would allow investigation of this relationship with better spatial precision.

6. Conclusion

Using sensitive high-resolution neuroimaging techniques, we showed that elevated relative AP is related to higher probability of WMHs, supporting the idea that damage to WM may lead to compensatory enhancement of rhythmic activity in the alpha frequency range. Importantly, our study provides evidence that the prevalence of regional WMHs, characterized by higher relative AP, was not associated with age *per se*, in fact, the latter seems to be mediated by total WMH volume. Our findings thus suggest that longitudinal EEG recordings might be sensitive for the detection of alterations in neuronal activities due to progressive structural changes in WM.

7. Acknowledgments

We thank all members of the Leipzig Research Center for Civilization Diseases (LIFE) study center for conducting the LIFE-Adult study and also all participants for their valuable collaboration.

8. Funding

This work is supported by the European Union, the European Regional Development Fund, and the Free State of Saxony within the framework of the excellence initiative and LIFE – Leipzig Research Center for Civilization Diseases, University of Leipzig.

SH is funded by the European Research Council (ERC) under the European Union's Horizon 2020 research and innovation programme (Grant agreement No. 758985).

9. Data availability

Anonymized data will be made available upon request through the application procedure carried out by the LIFE-Study administration (https://life.uni-leipzig.de/de/erwachsenen_kohorten/life_adult.html).

10. Disclosure statement

The authors report no conflict of interest.

11. References

Avants, B.B., Tustison, N.J., Song, G., Cook, P.A., Klein, A., Gee, J.C., 2011. A reproducible evaluation of ANTs similarity metric performance in brain image registration. Neuroimage 54, 2033–2044. https://doi.org/10.1016/j.neuroimage.2010.09.025

Babiloni, C., Frisoni, G.B., Pievani, M., Toscano, L., Del Percio, C., Geroldi, C., Eusebi, F., Miniussi, C., Rossini, P.M., 2008a. White-matter vascular lesions correlate with alpha EEG sources in mild cognitive impairment. Neuropsychologia 46, 1707–1720. https://doi.org/10.1016/j.neuropsychologia.2008.03.021

Babiloni, C., Frisoni, G.B., Pievani, M., Vecchio, F., Infarinato, F., Geroldi, C., Salinari, S., Ferri, R., Fracassi, C., Eusebi, F., Rossini, P.M., 2008b. White matter vascular lesions are related to parietal-to-frontal coupling of EEG rhythms in mild cognitive impairment. Hum. Brain Mapp. 29, 1355–1367. https://doi.org/10.1002/hbm.20467

Babiloni, C., Lizio, R., Carducci, F., Vecchio, F., Redolfi, A., Marino, S., Tedeschi, G., Montella, P., Guizzaro, A., Esposito, F., Bozzao, A., Giubilei, F., Orzi, F., Quattrocchi, C.C., Soricelli, A., Salvatore, E., Baglieri, A., Bramanti, P., Cavedo, E., Ferri, R., Cosentino, F., Ferrara, M., Mundi, C., Grilli, G., Pugliese, S., Gerardi, G., Parisi, L., Vernieri, F., Triggiani, A.I., Pedersen, J.T., Hrdemark, H.G., Rossini, P.M., Frisoni, G.B., 2011. Resting state cortical electroencephalographic rhythms and white matter vascular lesions in subjects with alzheimer's disease: An italian multicenter study. J. Alzheimer's Dis. 26, 331–346. https://doi.org/10.3233/JAD-2011-101710

Babiloni, C., Pievani, M., Vecchio, F., Geroldi, C., Eusebi, F., Fracassi, C., Fletcher, E., De Carli, C., Boccardi, M., Rossini, P.M., Frisoni, G.B., 2009. White-matter lesions along the cholinergic tracts are related to cortical sources of eeg rhythms in amnesic mild cognitive impairment. Hum. Brain Mapp. 30, 1431–1443. https://doi.org/10.1002/hbm.20612

Bazanova, O.M., Vernon, D., 2014. Interpreting EEG alpha activity. Neurosci. Biobehav. Rev. 44, 94–110. https://doi.org/10.1016/J.NEUBIOREV.2013.05.007

Bell, A.J., Sejnowski, T.J., 1995. An Information-Maximization Approach to Blind Separation and Blind Deconvolution. Neural Comput. 7, 1129–1159. https://doi.org/10.1162/neco.1995.7.6.1129

Birdsill, A.C., Koscik, R.L., Jonaitis, E.M., Johnson, S.C., Okonkwo, O.C., Hermann, B.P., LaRue, A., Sager, M.A., Bendlin, B.B., 2014. Regional white matter hyperintensities: Aging, Alzheimer's disease risk, and cognitive function. Neurobiol. Aging 35, 769–776. https://doi.org/10.1016/j.neurobiolaging.2013.10.072

477 Cabeza, R., Albert, M., Belleville, S., Craik, F.I.M., Duarte, A., Grady, C.L., Lindenberger,
478 U., Nyberg, L., Park, D.C., Reuter-Lorenz, P.A., Rugg, M.D., Steffener, J., Rajah, M.N.,
479 2018. Maintenance, reserve and compensation: the cognitive neuroscience of healthy
480 ageing. Nat. Rev. Neurosci. 19, 701–710. https://doi.org/10.1038/s41583-018-0068-2
481 Debette, S., Markus, H.S., 2010. The clinical importance of white matter hyperintensities on
482 brain magnetic resonance imaging: Systematic review and meta-analysis. BMJ 341, 288.
483 https://doi.org/10.1136/bmj.c3666
484 DeCarli, C., Fletcher, E., Ramey, V., Harvey, D., Jagust, W.J., 2005. Anatomical Mapping of
485 White Matter Hyperintensities (WMH). Stroke 36, 50–55.
486 https://doi.org/10.1161/01.str.0000150668.58689.f2
487 Desikan, R.S., Ségonne, F., Fischl, B., Quinn, B.T., Dickerson, B.C., Blacker, D., Buckner,
488 R.L., Dale, A.M., Maguire, R.P., Hyman, B.T., Albert, M.S., Killiany, R.J., 2006. An
489 automated labeling system for subdividing the human cerebral cortex on MRI scans into
490 gyral based regions of interest. Neuroimage 31, 968–980.
491 https://doi.org/10.1016/j.neuroimage.2006.01.021
492 Fields, R.D., 2015. A new mechanism of nervous system plasticity: Activity-dependent
493 myelination. Nat. Rev. Neurosci. 16, 756–767. https://doi.org/10.1038/nrn4023
494 Fields, R.D., 2008. White matter in learning, cognition and psychiatric disorders. Trends
495 Neurosci. 31, 361–370. https://doi.org/10.1016/j.tins.2008.04.001
496 Fischl, B., 2012. FreeSurfer. Neuroimage 62, 774–781.
497 https://doi.org/10.1016/j.neuroimage.2012.01.021
498 Fox, N.A., Yoo, K.H., Bowman, L.C., Cannon, E.N., Ferrari, P.F., Bakermans-Kranenburg,
499 M.J., Vanderwert, R.E., Van IJzendoorn, M.H., 2016. Assessing human mirror activity
500 With EEG mu rhythm: A meta-analysis. Psychol. Bull. 142, 291–313.
501 https://doi.org/10.1037/bul0000031
502 Gramfort, A., Papadopoulo, T., Olivi, E., Clerc, M., 2010. OpenMEEG: Opensource software
503 for quasistatic bioelectromagnetics. Biomed. Eng. Online 9.
504 https://doi.org/10.1186/1475-925X-9-45
505 Habes, M., Erus, G., Toledo, J.B., Zhang, T., Bryan, N., Launer, L.J., Rosseel, Y., Janowitz,
506 D., Doshi, J., Van Der Auwera, S., Von Sarnowski, B., Hegenscheid, K., Hosten, N.,
507 Homuth, G., Völzke, H., Schminke, U., Hoffmann, W., Grabe, H.J., Davatzikos, C.,
508 2016. White matter hyperintensities and imaging patterns of brain ageing in the general
509 population. Brain 139, 1164–1179. https://doi.org/10.1093/brain/aww008
510 Hardstone, R., Poil, S.S., Schiavone, G., Jansen, R., Nikulin, V. V., Mansvelder, H.D.,

511 Linkenkaer-Hansen, K., 2012. Detrended fluctuation analysis: A scale-free view on
512 neuronal oscillations. Front. Physiol. 3 NOV. https://doi.org/10.3389/fphys.2012.00450
513 Hinault, T., Kraut, M., Bakker, A., Dagher, A., Courtney, S.M., 2020. Disrupted Neural
514 Synchrony Mediates the Relationship between White Matter Integrity and Cognitive
515 Performance in Older Adults. Cereb. Cortex 1–13.
516 https://doi.org/10.1093/cercor/bhaa141
517 Hindriks, R., van Putten, M.J.A.M., 2013. Thalamo-cortical mechanisms underlying changes
518 in amplitude and frequency of human alpha oscillations. Neuroimage 70, 150–163.
519 https://doi.org/10.1016/j.neuroimage.2012.12.018
520 Hindriks, R., Woolrich, M., Luckhoo, H., Joensson, M., Mohseni, H., Kringelbach, M.L.,
521 Deco, G., 2015. Role of white-matter pathways in coordinating alpha oscillations in
522 resting visual cortex. Neuroimage 106, 328–339.
523 https://doi.org/10.1016/j.neuroimage.2014.10.057
524 Hochberg, Y., 2016. Controlling the False Discovery Rate : A Practical and Powerful
525 Approach to Multiple Testing. J. R. Stat. Soc. 57, 289–300.
526 Ishii, R., Canuet, L., Aoki, Y., Hata, M., Iwase, M., Ikeda, S., Nishida, K., Ikeda, M., 2018.
527 Healthy and Pathological Brain Aging: From the Perspective of Oscillations, Functional
528 Connectivity, and Signal Complexity. Neuropsychobiology 0871.
529 https://doi.org/10.1159/000486870
530 Jawinski, P., Kittel, J., Sander, C., Huang, J., Spada, J., Ulke, C., Wirkner, K., Hensch, T.,
531 Hegerl, U., 2017. Recorded and reported sleepiness: The association between brain
532 arousal in resting state and subjective daytime sleepiness. Sleep 40.
533 https://doi.org/10.1093/sleep/zsx099
534 Jenkinson, M., Beckmann, C.F., Behrens, T.E.J., Woolrich, M.W., Smith, S.M., 2012. Fsl.
535 Neuroimage 62, 782–790. https://doi.org/10.1016/j.neuroimage.2011.09.015
536 Klimesch, W., 1999. EEG alpha and theta oscillations reflect cognitive and memory
537 performance: A review and analysis. Brain Res. Rev. 29, 169–195.
538 https://doi.org/10.1016/S0165-0173(98)00056-3
539 Knyazeva, M.G., Barzegaran, E., Vildavski, V.Y., Demonet, J.F., 2018. Aging of human
540 alpha rhythm. Neurobiol. Aging 69, 261–273.
541 https://doi.org/10.1016/j.neurobiolaging.2018.05.018
542 Lampe, L., Zhang, R., Beyer, F., Huhn, S., Kharabian Masouleh, S., Preusser, S., Bazin, P.L.,
543 Schroeter, M.L., Villringer, A., Witte, A.V., 2019. Visceral obesity relates to deep white
544 matter hyperintensities via inflammation. Ann. Neurol. 85, 194–203.

https://doi.org/10.1002/ana.25396

Leunissen, I., Coxon, J.P., Caeyenberghs, K., Michiels, K., Sunaert, S., Swinnen, S.P., 2014. Task switching in traumatic brain injury relates to cortico-subcortical integrity. Hum. Brain Mapp. 35, 2459–2469. https://doi.org/10.1002/hbm.22341

Linkenkaer-Hansen, K., Nikouline, V. V., Palva, J.M., Ilmoniemi, R.J., 2001. Long-range temporal correlations and scaling behavior in human brain oscillations. J. Neurosci. 21, 1370–1377. https://doi.org/10.1523/jneurosci.21-04-01370.2001

Loeffler, M., Engel, C., Ahnert, P., Alfermann, D., Arelin, K., Baber, R., Beutner, F., Binder, H., Brähler, E., Burkhardt, R., Ceglarek, U., Enzenbach, C., Fuchs, M., Glaesmer, H., Girlich, F., Hagendorff, A., Häntzsch, M., Hegerl, U., Henger, S., Hensch, T., Hinz, A., Holzendorf, V., Husser, D., Kersting, A., Kiel, A., Kirsten, T., Kratzsch, J., Krohn, K., Luck, T., Melzer, S., Netto, J., Nüchter, M., Raschpichler, M., Rauscher, F.G., Riedel-Heller, S.G., Sander, C., Scholz, M., Schönknecht, P., Schroeter, M.L., Simon, J.C., Speer, R., Stäker, J., Stein, R., Stöbel-Richter, Y., Stumvoll, M., Tarnok, A., Teren, A., Teupser, D., Then, F.S., Tönjes, A., Treudler, R., Villringer, A., Weissgerber, A., Wiedemann, P., Zachariae, S., Wirkner, K., Thiery, J., 2015. The LIFE-Adult-Study: Objectives and design of a population-based cohort study with 10,000 deeply phenotyped adults in Germany. BMC Public Health 15, 691. https://doi.org/10.1186/s12889-015-1983-z

Lopes Da Silva, F.H., Pijn, J.P., Velis, D., Nijssen, P.C.G., 1997. Alpha rhythms: Noise, dynamics and models. Int. J. Psychophysiol. 26, 237–249. https://doi.org/10.1016/S0167-8760(97)00767-8

Madden, D.J., Parks, E.L., Tallman, C.W., Boylan, M.A., Hoagey, D.A., Cocjin, S.B., Packard, L.E., Johnson, M.A., Chou, Y. hui, Potter, G.G., Chen, N. kuei, Siciliano, R.E., Monge, Z.A., Honig, J.A., Diaz, M.T., 2017. Sources of disconnection in neurocognitive aging: cerebral white-matter integrity, resting-state functional connectivity, and white-matter hyperintensity volume. Neurobiol. Aging 54, 199–213. https://doi.org/10.1016/j.neurobiolaging.2017.01.027

Mahjoory, K., Cesnaite, E., Hohlefeld, F.U., Villringer, A., Nikulin, V. V., 2019. Power and temporal dynamics of alpha oscillations at rest differentiate cognitive performance involving sustained and phasic cognitive control. Neuroimage 188, 135–144. https://doi.org/10.1016/j.neuroimage.2018.12.001

Mierau, A., Klimesch, W., Lefebvre, J., 2017. State-dependent alpha peak frequency shifts: Experimental evidence, potential mechanisms and functional implications. Neuroscience

360, 146–154. https://doi.org/10.1016/j.neuroscience.2017.07.037

Minami, S., Oishi, H., Takemura, H., Amano, K., 2020. Inter-individual differences in occipital alpha oscillations correlate with white matter tissue properties of the optic radiation. Eneuro ENEURO.0224-19.2020. https://doi.org/10.1523/eneuro.0224-19.2020

Nikulin, V. V., Brismar, T., 2005. Long-range temporal correlations in electroencephalographic oscillations: Relation to topography, frequency band, age and gender. Neuroscience 130, 549–558. https://doi.org/10.1016/j.neuroscience.2004.10.007

O'Sullivan, M., Jones, D.K., Summers, P.E., Morris, R.G., Williams, S.C.R., Markus, H.S., 2001. Evidence for cortical "disconnection" as a mechanism of age-related cognitive decline. Neurology 57, 632–638. https://doi.org/10.1212/WNL.57.4.632

Pascual-Marqui, R.D., 2007. Discrete, 3D distributed, linear imaging methods of electric neuronal activity. Part 1: exact, zero error localization.

Pfurtscheller, G., Lopes Da Silva, F.H., 1999. Event-related EEG/MEG synchronization and desynchronization: Basic principles. Clin. Neurophysiol. 110, 1842–1857. https://doi.org/10.1016/S1388-2457(99)00141-8

Poil, S.-S., Hardstone, R., Mansvelder, H.D., Linkenkaer-Hansen, K., 2012. Critical-State Dynamics of Avalanches and Oscillations Jointly Emerge from Balanced Excitation/Inhibition in Neuronal Networks. J. Neurosci. 32, 9817–9823. https://doi.org/10.1523/jneurosci.5990-11.2012

Ryu, S.Y., Coutu, J.P., Rosas, H.D., Salat, D.H., 2014. Effects of insulin resistance on white matter microstructure in middle-aged and older adults. Neurology 82, 1862–1870. https://doi.org/10.1212/WNL.0000000000000452

Sahoo, B., Pathak, A., Deco, G., Banerjee, A., Roy, D., 2020. Lifespan associated global patterns of coherent neural communication. Neuroimage 216, 116824. https://doi.org/10.1016/j.neuroimage.2020.116824

Samek, W., Blythe, D.A.J., Curio, G., Müller, K.R., Blankertz, B., Nikulin, V. V., 2016. Multiscale temporal neural dynamics predict performance in a complex sensorimotor task. Neuroimage 141, 291–303. https://doi.org/10.1016/j.neuroimage.2016.06.056

Scally, B., Burke, M.R., Bunce, D., Delvenne, J.F., 2018. Resting-state EEG power and connectivity are associated with alpha peak frequency slowing in healthy aging. Neurobiol. Aging 71, 149–155. https://doi.org/10.1016/j.neurobiolaging.2018.07.004

Shew, W.L., Plenz, D., 2013. The functional benefits of criticality in the cortex. Neuroscientist 19, 88–100. https://doi.org/10.1177/1073858412445487

Shiee, N., Bazin, P.L., Ozturk, A., Reich, D.S., Calabresi, P.A., Pham, D.L., 2010. A

613 topology-preserving approach to the segmentation of brain images with multiple
614 sclerosis lesions. Neuroimage 49, 1524–1535.
615 https://doi.org/10.1016/j.neuroimage.2009.09.005
616 Smit, D.J.A., de Geus, E.J.C., van de Nieuwenhuijzen, M.E., van Beijsterveldt, C.E.M., van
617 Baal, G.C.M., Mansvelder, H.D., Boomsma, D.I., Linkenkaer-Hansen, K., 2011. Scale-
618 Free Modulation of Resting-State Neuronal Oscillations Reflects Prolonged Brain
619 Maturation in Humans. J. Neurosci. 31, 13128–13136.
620 https://doi.org/10.1523/JNEUROSCI.1678-11.2011
621 Smith, C.D., Snowdon, D.A., Wang, H., Markesbery, W.R., 2000. White matter volumes and
622 periventricular white matter hyperintensities in aging and dementia. Neurology 54, 838–
623 842. https://doi.org/10.1212/WNL.54.4.838
624 Suffczynski, P., Kalitzin, S., Pfurtscheller, G., Lopes Da Silva, F.H., 2001. Computational
625 model of thalamo-cortical networks: Dynamical control of alpha rhythms in relation to
626 focal attention. Int. J. Psychophysiol. 43, 25–40. https://doi.org/10.1016/S0167-
627 8760(01)00177-5
628 Tingley, D., Yamamoto, T., Hirose, K., Keele, L., Imai, K., 2014. Mediation: R package for
629 causal mediation analysis. J. Stat. Softw. 59, 1–38. https://doi.org/10.18637/jss.v059.i05
630 Valdés-Hernández, P.A., Ojeda-González, A., Martínez-Montes, E., Lage-Castellanos, A.,
631 Virués-Alba, T., Valdés-Urrutia, L., Valdes-Sosa, P.A., 2010. White matter architecture
632 rather than cortical surface area correlates with the EEG alpha rhythm. Neuroimage 49,
633 2328–2339. https://doi.org/10.1016/j.neuroimage.2009.10.030
634 van Straaten, E.C.W., de Haan, W., de Waal, H., Scheltens, P., van der Flier, W.M., Barkhof,
635 F., Koene, T., Stam, C.J., 2012. Disturbed oscillatory brain dynamics in subcortical
636 ischemic vascular dementia. BMC Neurosci. 13. https://doi.org/10.1186/1471-2202-13-
637 85
638 Wardlaw, J.M., Valdés Hernández, M.C., Muñoz-Maniega, S., 2015. What are white matter
639 hyperintensities made of? Relevance to vascular cognitive impairment. J. Am. Heart
640 Assoc. 4, 001140. https://doi.org/10.1161/JAHA.114.001140
641 Winkler, A.M., Ridgway, G.R., Webster, M.A., Smith, S.M., Nichols, T.E., 2014.
642 Permutation inference for the general linear model. Neuroimage 92, 381–397.
643 https://doi.org/10.1016/j.neuroimage.2014.01.060
644

Supplementary Material

All variables are presented as mean (M) ± standard deviation (SD). Before the statistical analyses, we used the Box-Cox method (λ value) (Sakia, 1992) to determine the type transformation on the parameters of alpha oscillations. Since the majority of the variables after the necessary transformation did not pass Shapiro-Wilk normality tests at the 0.05 significance level, we decided to keep the original values.

Supplementary Figure 1. The four histograms show the distribution of **A)** total white matter hyperintensity (WMH), **B)** averaged individual alpha peak frequency (IAPF), **C)** relative alpha power, and **D)** long-range temporal correlation (LRTC) across 31 EEG channels.

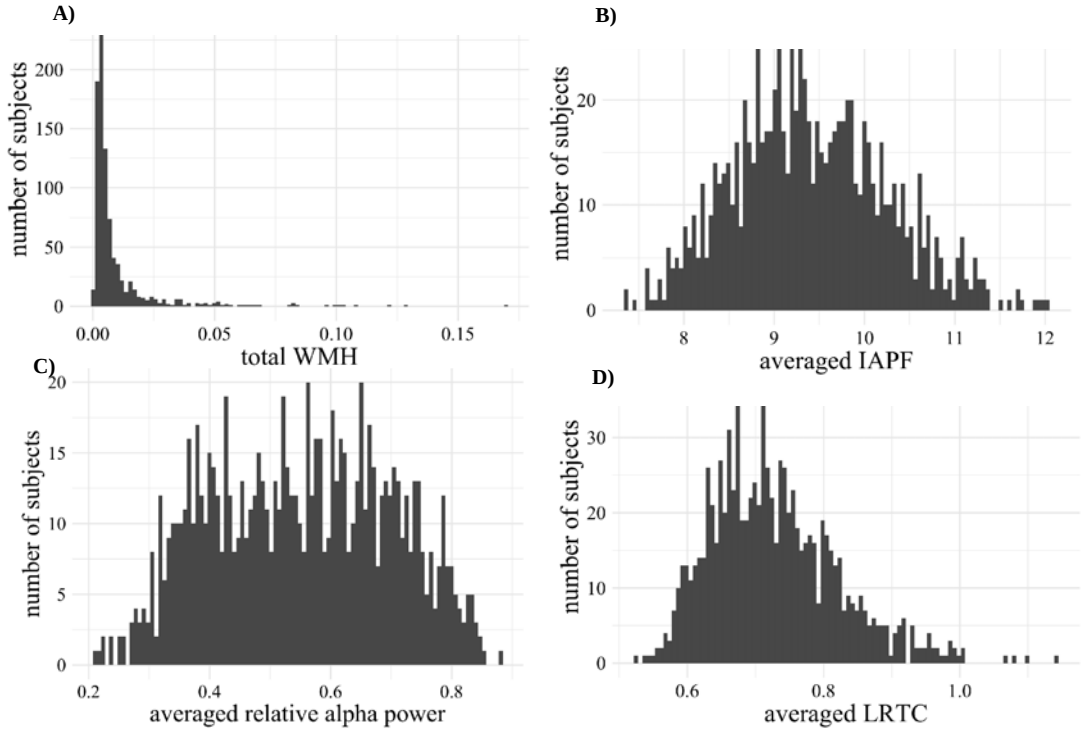

Supplementary Figure 2. Grand-average topographic maps of alpha band measures in EEG.

A) Individual alpha peak frequency; **B)** Relative alpha power; **C)** Long-range temporal correlations. **D)** Grand-average of relative alpha power at EEG source space across 68 regions based on Desikan-Killiany Atlas.

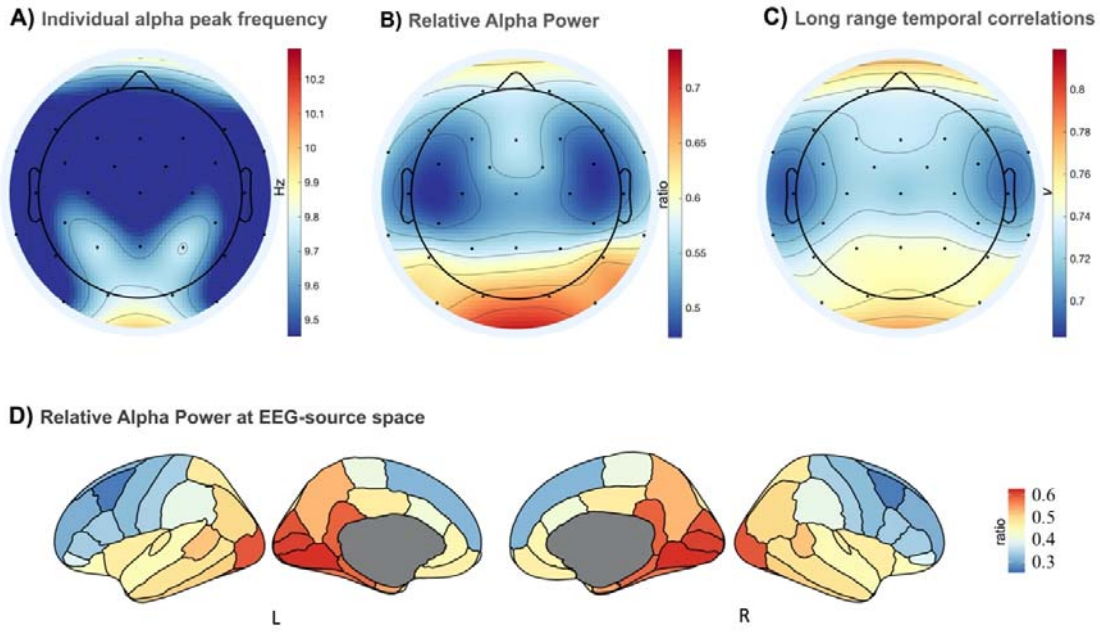

Supplementary Figure 3. Association between age (x-axis) and total white matter hyperintensity (WMH, y-axis) in LIFE-Adult sample (N=907). There was a significant correlation between age and total WMH (overall, $r = 0.374$, $p < 0.001$; females, $r = 0.376$, $p < 0.001$; males, $r = 0.355$, $p < 0.001$)

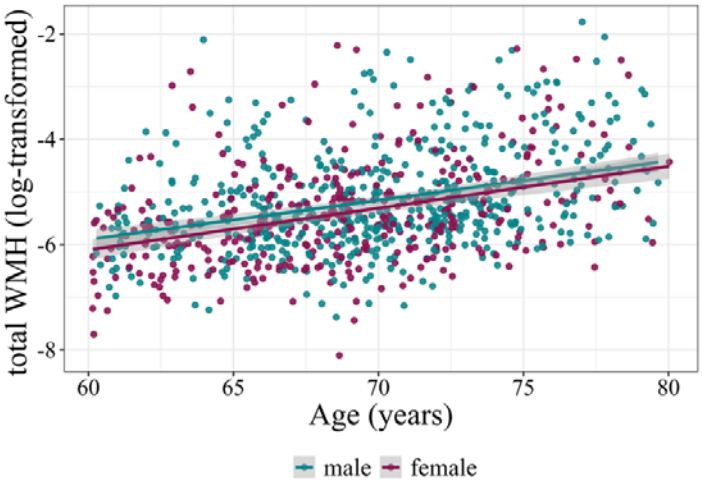

Supplementary Figure 4. Association between age (x-axis) and regional white matter hyperintensity as the ratio of deep WMH and periventricular WMH (y-axis) in LIFE-Adult sample (N=907) (overall, r = 0.03; females, r = -0.005; males, r = 0.038, p >0.05)

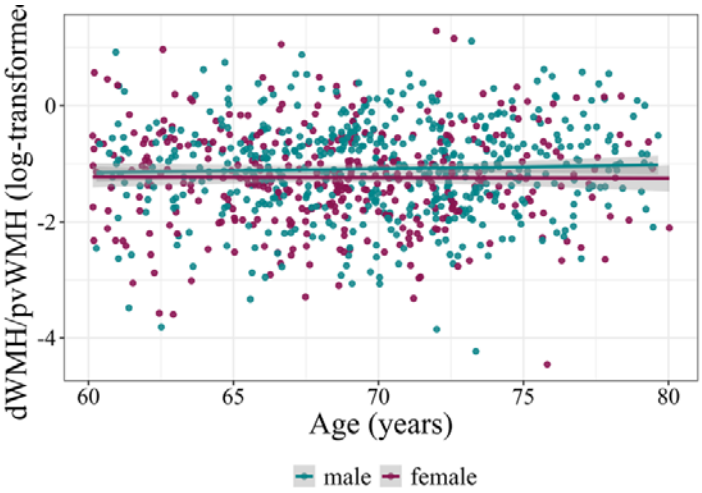

Supplementary Figure 5. Association between age (x-axis) and individual alpha peak frequency (IAPF, y-axis) in EEG different regions. The correlations between two measures were significant after FDR correction (frontal, r = -0.17, females, r = -0.15, males, r = -0.16; central, r = -0.14; females, r = -0.13, males, r = -0.13, left temporal, r = -0.17, females, r = -0.17, males, r = -0.17; right temporal, r = -0.16, females, r = -0.14; males, r = -0.16; parietal, r = -0.15, females, r = -0.15, males, r = -0.13; occipital, r = -0.17, females, r = -0.15, males, r = -0.15). None of the pairwise correlations differed from each other. Abbr.: F- female, M-male

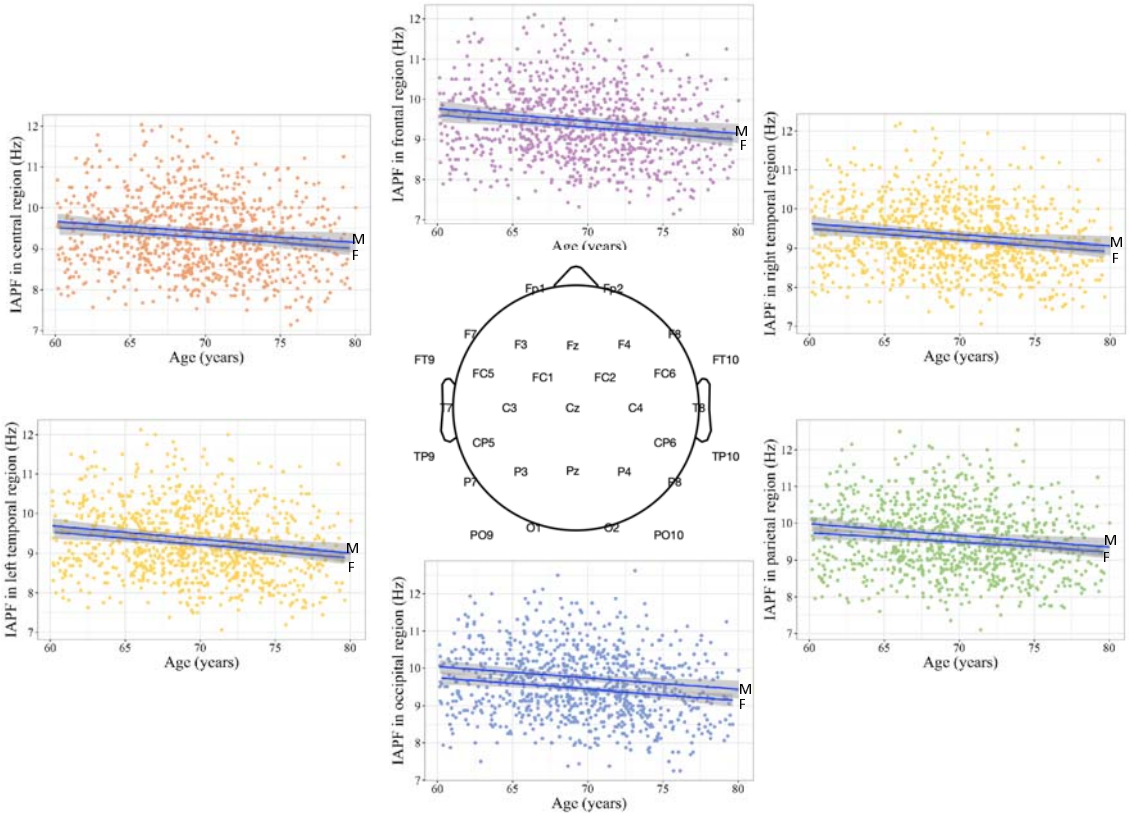

Supplementary Figure 6. Association between age (x-axis) and relative alpha power (y-axis) in different EEG regions. The correlations between two measures were not significant after FDR correction (frontal, r = 0.010, females, r = -0.008, males, r = 0.008; central, r = 0.010; females, r = 0.019, males, r = 0.012, left temporal, r = 0.068, females, r = 0.098, males, r = 0.027; right temporal, r = 0.071, females, r = 0.090; males, r = 0.040; parietal, r = 0.03, females, r = 0.03, males, r = 0.02; occipital, r = 0.016, females, r = 0.001, males, r = 0.016). None of the pairwise correlations differed from each other. Abbr.: F- female, M-male

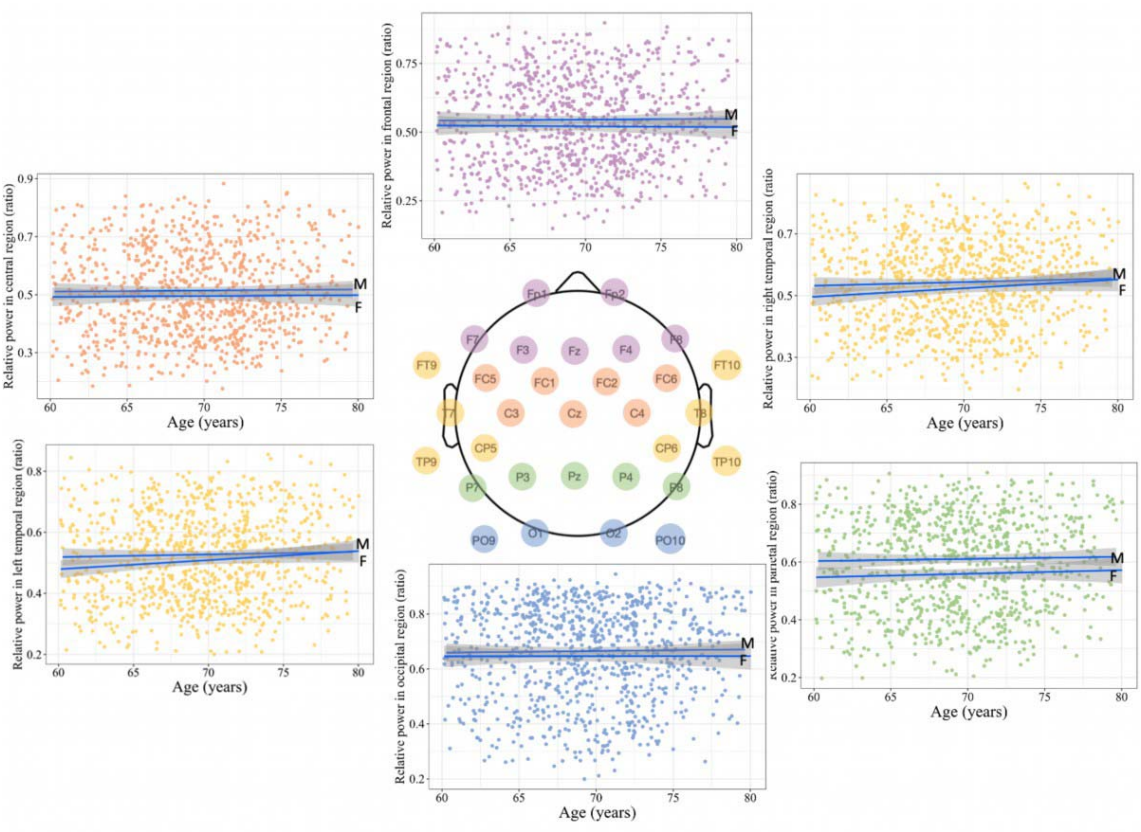

Supplementary Figure 7. Association between age (x-axis) and scaling exponent for long-range temporal correlations (LRTC, y-axis) in different EEG regions. Association between age (x-axis) and relative alpha power (y-axis) in different regions (represented in different colors). The correlations between two measures were not significant after FDR correction (frontal, r = -0.02, females, r = -0.04, males, r = -0.04; central, r = -0.03; females, r = -0.05, males, r = -0.04, left temporal, r = -0.02, females, r = -0.04, males, r = -0.05; right temporal, r = -0.04, females, r = -0.06; males, r = -0.07; parietal, r = -0.05, females, r = -0.04, males, r = -0.06; occipital, r = -0.02, females, r = -0.03, males, r = -0.03). None of the pairwise correlations differed from each other. Abbr.: F- female, M-male

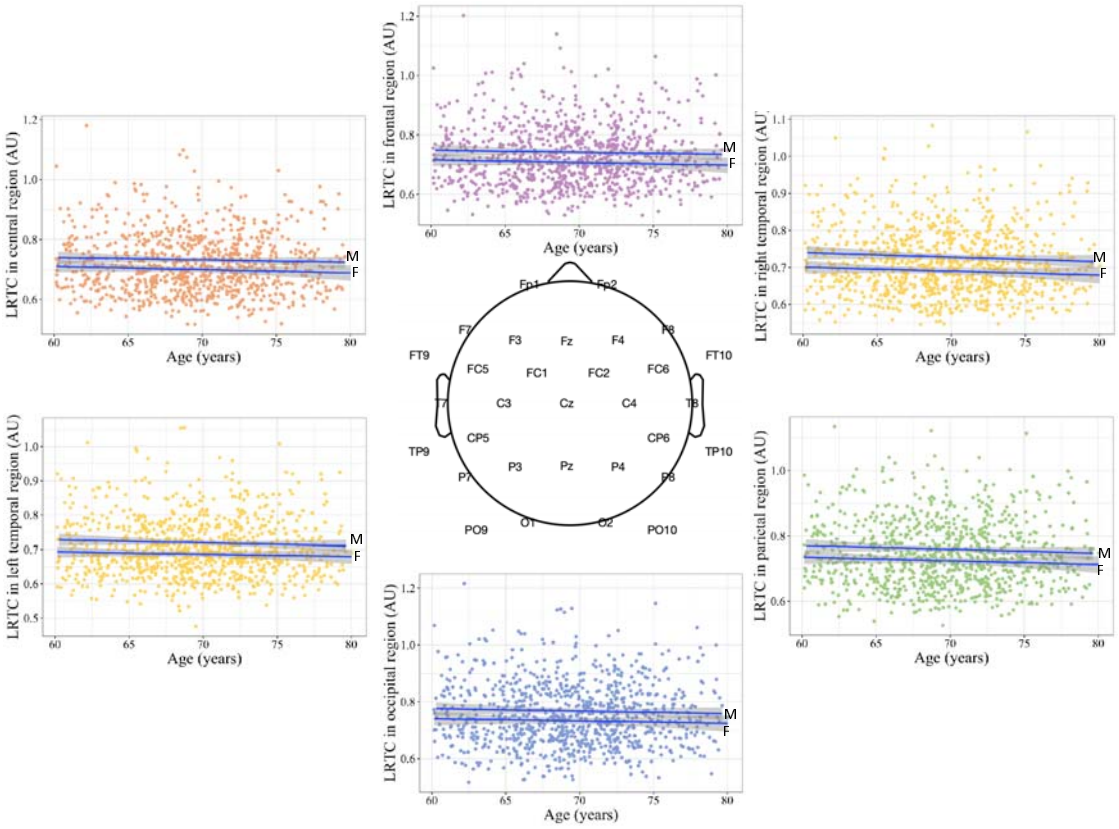

Supplementary Table 1 – Mediation effect of total WMH volume on the association between age and relative alpha power at EEG sensor space. Significant pathways are marked in bold.

EEG Region	**frontal**		**central**		**right temporal**		**left temporal**		**parietal**		**occipital**	
	β	p or 99.5% CI	β	p or 99.5% CI	β	p or 99.5% CI	β	p or 99.5% CI	β	p or 99.5% CI	β	p or 99.5% CI
Total effect c (Age on rel. AP)	0.0004	0.742	0.0006	0.58	**0.002**	**0.03**	0.002	0.0620	0.0017	0.166	0.0006	0.584
Mediation effect a*b (Age on rel. AP via total WMH)	0.0009	[-0.0003, 0.0021]	0.001	[-0.00008, 0.0022]	**0.0013**	**[0.0003, 0.02]**	**0.0011**	**[0.00002, 0.002]**	**0.0015**	**[0.0002, 0.0028]**	**0.0014**	**[0.00012, 0.0029]**
Direct effect c' (Age on rel. AP)	-0.0005	0.721	-0.0004	0.73	0.0008	0.44	0.0009	0.3944	0.0002	0.894	-0.0008	0.557

Abbreviations.: rel AP = Relative Alpha Power; CI = Confidence Interval; WMH = White matter hyperintensity